

# Optimized Hamiltonian learning from short-time measurements

Assaf Zubida, Elad Yitzhaki, Netanel H. Lindner, and Eyal Bairey\*  
*Physics Department, Technion, 3200003, Haifa, Israel*

Characterizing noisy quantum devices requires methods for learning the underlying quantum Hamiltonian which governs their dynamics. Often, such methods compare measurements to simulations of candidate Hamiltonians, a task which requires exponential computational complexity. Here, we analyze and optimize a method which circumvents this difficulty using measurements of short time dynamics. We provide estimates for the optimal measurement schedule and reconstruction error. We demonstrate that the reconstruction requires a system-size independent number of experimental shots, and characterize an informationally-complete set of state preparations and measurements for learning local Hamiltonians. Finally, we show how grouping of commuting observables and use of Hamiltonian symmetries can improve the Hamiltonian reconstruction.

*Introduction.* Recovering the unknown Hamiltonian of a quantum system is becoming an increasingly important task for modelling quantum materials [1, 2], characterizing quantum states [3–8] and engineering quantum devices [9–12]. Whereas benchmarking protocols can extract the average error rates of quantum devices [13], Hamiltonian learning provides a detailed characterization of their real-time dynamics, allowing to identify physical sources of errors [14–16].

Many Hamiltonian learning methods are based on measurements of time-dependent observables in quantum states evolved over time [17–23]. However, as time progresses, the dynamics of many-body Hamiltonians become exponentially complex, posing a computational challenge when attempting to find the Hamiltonian which matches the observed behaviour. To deal with this exponential complexity, some approaches assume partial control of the quantum system to be characterized [24–27], or employ an additional trusted quantum simulator [28–32]. Alternatively, methods based on energy conservation search for a local operator whose expectation value does not change in time; these methods can recover Hamiltonians without symmetries with a complexity which scales polynomially with system size [33, 34]. Here the complexity refers both to the number of measurements and the classical computation involved in the learning procedure.

A promising approach which avoids this complexity learns Hamiltonians from short-time dynamics [35, 36]. This approach learns short-ranged Hamiltonians by preparing various product states, and measuring the time-derivative of different observables [36]. The short-time dynamics are linear in the Hamiltonian parameters, allowing a computationally-efficient reconstruction. The rapid experimental preparation of product states provides an advantage over approaches which learn the dynamics from their steady states [37–47].

Here we optimize measurement protocols for learning short-ranged Hamiltonians from short time dynamics. We analyze numerically the reconstruction error in a protocol that prepares random product states and mea-

sures in random local bases, as in recent randomized measurement protocols [34, 46, 48, 49]. We then propose a derandomized protocol that guarantees the same reconstruction accuracy with a fixed set of initial states and measurements. For a given state, the measurements of this protocol characterize all geometrically-local reduced density matrices using a fixed set of measurement bases, adapting overlapping tomography methods [50–52] to the special case of lattices. Our analysis shows that the total number of measurements required to recover a short-ranged Hamiltonian to a fixed accuracy is in fact system-size independent. Importantly, it provides an accurate numerical estimate for the optimal measurement time based on a rough prior guess of the Hamiltonian.

*Problem setting.* The goal of the scheme we analyze is to recover short-ranged Hamiltonians from their short-time dynamics [36]. We say that a closed quantum system on a lattice is governed by a  $k$ -ranged Hamiltonian if each term in the Hamiltonian is contained in a cube of side length  $k$ . The procedure for learning a  $k$ -ranged Hamiltonian  $H$  consists of (i) initializing the system in different product states  $|\psi\rangle$ , (ii) evolving the initial states for a short time under  $H$ , and (iii) measuring the evolved states in various bases. Our goal is to reconstruct  $H$  to a given accuracy using a minimal number of shots  $N$ , defined as the total number of experiments, from state preparation to measurement. Both the number of shots and the classical computation should scale favourably with the size of the system.

Any  $k$ -ranged Hamiltonian  $H$  may be expanded in a basis  $\{S_j\}$  for the space of  $k$ -ranged operators,

$$H = \sum_j c_j S_j, \quad (1)$$

such that the Hamiltonian is determined by the coefficients  $c_j$ . The reconstruction of  $H$  then boils down to finding the coefficient vector  $\vec{c}$ . For concreteness, we describe the reconstruction algorithm for spin  $1/2$  systems, where  $S_j$  are products of Paulis acting on contiguous sites. While we describe it for closed system, the algorithm can also recover the dynamics of a subsystem embedded in a larger system as in Ref. [43], as well as Markovian dissipative dynamics as in Refs. [44, 45].

\* [baeyal@gmail.com](mailto:baeyal@gmail.com)

*Algorithm.* The dynamics of an observable  $A$  in an initial state  $|\psi\rangle$  is governed by Ehrenfest's equation,

$$\partial_t \langle A \rangle_\psi = i \langle [H, A] \rangle_\psi = i \sum_j c_j \langle [S_j, A] \rangle_\psi, \quad (2)$$

where  $\langle A \rangle_\psi = \langle \psi | A | \psi \rangle$ . For a known initial state  $|\psi\rangle$  at  $t = 0$ , Eq. (2) yields an equation for the Hamiltonian coefficients  $c_j$ . We can get a set of equations using different pairs of initial states  $\{|\psi_\alpha\rangle\}$  and observables  $\{A_\beta\}$ . Denoting

$$b_{(\alpha, \beta)} \stackrel{\text{def}}{=} \partial_t \langle A_\beta \rangle_{\psi_\alpha}, \quad K_{(\alpha, \beta), j} \stackrel{\text{def}}{=} i \langle [S_j, A_\beta] \rangle_{\psi_\alpha}, \quad (3)$$

where we treat the pair  $(\alpha, \beta)$  as a super index, Eq. (2) becomes

$$b_{(\alpha, \beta)} = \sum_j K_{(\alpha, \beta), j} c_j, \quad (4)$$

yielding a set of linear equations

$$\vec{b} = K \vec{c}. \quad (5)$$

With sufficiently many initial states and observables,  $K$  becomes full rank, and the Hamiltonian  $\vec{c}$  is uniquely given by the solution  $\vec{c} = K^+ \vec{b}$ , where  $K^+ = (K^T K)^{-1} K^T$  is the pseudo inverse of  $K$ .

As can be seen in Eq. (5), the matrix  $K$  maps Hamiltonians to observable dynamics. The matrix does not depend on the unknown Hamiltonian, and can be calculated in advance given a set of initial states and observables. The observable dynamics  $\vec{b}$  contain information about  $H$ , and must be estimated from measurements to recover  $H$ . Each entry  $b_j$  is a derivative which can be approximated by a forward finite difference method,

$$\partial_t \langle A \rangle_\psi = \frac{\langle A \rangle_{\psi(\delta t)} - \langle A \rangle_{\psi(0)}}{\delta t} + \mathcal{O}(\delta t). \quad (6)$$

Starting with a known initial state, the only term we need to measure is  $\langle A \rangle_{\psi(\delta t)}$ , which we can evaluate by measuring  $|\psi(\delta t)\rangle$  in a basis compatible with  $A$ , as we now explain.

To construct a set of equations, we initialize the system with random Pauli eigenstates and measure by projecting on random Pauli bases. We initialize

$$|\psi(0)\rangle = \prod_i |\phi_i\rangle, \quad (7)$$

where each  $\phi_i$  is chosen uniformly from one of the six  $\pm 1$  eigenstates of  $X, Y$  and  $Z$ . We propagate  $|\psi\rangle$  under  $H$  for a time  $\delta t$ . We then measure each site of  $|\psi(\delta t)\rangle$  randomly in one of the 3 Pauli bases  $X, Y$  or  $Z$ . Namely, we measure  $R^\dagger |\psi(\delta t)\rangle$  in the standard ( $Z$ ) basis, where  $R = \prod_i R_i$  and  $R_i$  are chosen uniformly from  $R_y(\pi/2), R_x(\pi/2)$ , and  $\mathbb{1}$ . We call each choice of state preparation and measurement basis a SPAM setting, and

denote the number of different SPAM settings used for reconstruction by  $N_{\text{spam}}$ .

In a system with  $n$  sites, each SPAM setting potentially contributes  $2^n - 1$  equations to the set (5), corresponding to  $\partial_t \langle A \rangle_\psi$  for commuting Pauli observables  $A$ . For instance, consider a measurement in the  $XZZX$  basis, which allows to estimate the single-site observables  $\langle X_1 \rangle, \langle Z_2 \rangle$  and so on at  $|\psi(\delta t)\rangle$ . Moreover, it allows to estimate the two-site correlators  $\langle X_1 Z_2 \rangle$  as well as higher-order correlators. Fixing a set of  $N_{\text{spam}}$  different SPAM settings yields a system (5) with up to  $\approx N_{\text{spam}} \cdot 2^n$  equations. In practice, we only estimate observables up to a given range  $k_\beta$ , corresponding to  $\approx n \cdot 2^{k_\beta - 1}$  equations per SPAM setting ( $2^{k_\beta - 1}$  correlators extending from each site, up to boundary corrections). Collecting a total of  $N$  shots distributed equally among the  $N_{\text{spam}}$  settings allows to estimate each of these equations to accuracy

$$\sim \frac{1}{\sqrt{N_{\text{spam}}/N}} = \sqrt{\frac{N_{\text{spam}}}{N}}.$$

This scheme raises a few questions, which we now address:

1. What is the optimal measurement time  $\delta t$ ?
2. How many experiments are needed to recover a short-ranged Hamiltonian to a given accuracy?
3. How does the number of required experiments depend on the system size?
4. Which observables should we estimate from each measurement setting?

*Estimating the reconstruction error and optimal measurement time.* We start by simulating our reconstruction algorithm on spin chains with random 2-ranged interactions, using single-site observables. To this end, we generated Hamiltonians with nearest neighbor Paulis  $S_j$ ,

$$H_{\text{random}} = \sum_j c_j S_j, \quad (8)$$

where  $S_j \in \{\sigma_i \otimes \sigma_{i+1}\}$  form a basis for all nearest neighbor Paulis, with  $\sigma_i \in \{\mathbb{1}_i, X_i, Y_i, Z_i\}$  a Pauli operator on site  $i$ . The coefficients were drawn from a Gaussian distribution with zero mean and unit variance  $c_j \sim G(0, 1)$ , setting the time scale for what follows. We initialized each system in  $N_{\text{spam}} = 648$  random product states [Eq. (7)], and evolved them for time  $\delta t$ . We measured each evolved state  $N/N_{\text{spam}}$  times in a random measurement basis, and estimated the expectation values of all single-site Paulis  $\langle A_\beta \rangle_{\psi(\delta t)}$  compatible with that basis from the measurement results. We then reconstructed the Hamiltonian coefficients  $\vec{c}$  from Eq. (5), approximating the time-derivative of each observable using finite differences [Eq. (6)].

Reconstructing a random Hamiltonian using various evolution times  $\delta t$  and a fixed measurement budget  $N = 10^6$ , the reconstruction error was minimized at an optimal measurement time  $\delta t^* \approx 0.02$  (Fig. 1, left). We

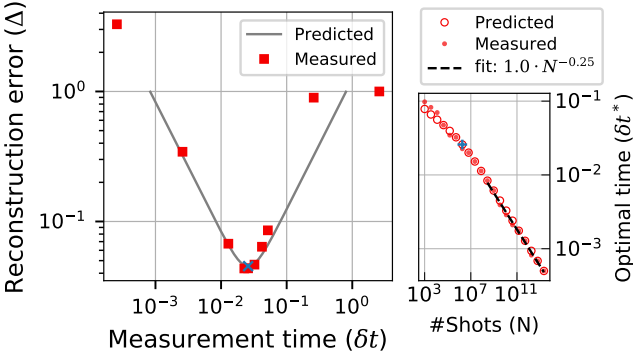


FIG. 1. Tradeoff between statistical and systematic errors determines optimal measurement time. Left: reconstruction error  $\Delta$  of a random 2-ranged Hamiltonian as a function of the measurement time  $\delta t$  for a fixed measurement budget  $N = 10^6$ . While the statistical error in the finite difference method decreases with  $\delta t$ , the systematic error increases with  $\delta t$ , dictating an optimal measurement time (blue circle). A prior estimate of the reconstruction error (gray line), calculated using a noisy guess of the Hamiltonian [Eq. (15)], predicts the optimal time (blue 'x'). Time is measured in units of the variance of the Hamiltonian couplings [see Eq. (8)]. Right: optimal measurement time  $\delta t^*$  as a function of the number of shots  $N$  (dots measured, circles predicted). The dashed line is a fit to the asymptotic scaling  $\delta t^* \sim N^{-\gamma}$  with  $\gamma \approx 1/4$ . The reported values average over 10 different realizations of the statistical estimation error for the observables; errorbars are smaller than the markers.

define the reconstruction error as the relative error of the reconstructed coefficients,

$$\Delta \stackrel{\text{def}}{=} \frac{\|\delta \vec{c}\|}{\|\vec{c}\|}. \quad (9)$$

Away from the optimal time, the reconstruction error increased significantly. Repeating the reconstruction with various measurement budgets  $N$ , the optimal measurement time  $\delta t^*$  scaled as  $N^{-1/4}$  (Fig. 1, right, dots). Can we predict the optimal measurement time  $\delta t^*$  and its reconstruction error  $\Delta^*$ ?

The accuracy of the Hamiltonian reconstruction from Eq. (5) is determined by the estimation accuracy of  $\vec{b}$ . In any experiment, instead of the exact  $\vec{b}$  we can only obtain a noisy estimate  $\vec{b} + \delta \vec{b}$ . The estimation error  $\delta \vec{b}$  corrupts the recovered coefficients, given by  $\vec{c} + \delta \vec{c} = K^+ (\vec{b} + \delta \vec{b})$ . This leads to an error in the reconstructed Hamiltonian, such that the deviation between the true and the recovered coefficients is given by  $\delta \vec{c} = K^+ \delta \vec{b}$ .

The error  $\delta \vec{b}$  in estimating the time-derivatives from Eq. (6) arises due to two factors: the finite measurement budget (the total number of experimental shots) and the finite-time approximation of the derivative. The finite sampling of  $\frac{\langle A(\delta t) \rangle}{\delta t}$  leads to statistical error which decreases with the number of experiments and measurement time,  $\|\delta \vec{b}_{\text{stat}}\| \sim \frac{1}{\sqrt{N \delta t}}$  (for a fixed  $N_{\text{spam}}$ ). The

finite-time approximation of the derivative leads to a systematic error which increases with time,  $\|\delta \vec{b}_{\text{sys}}\| \sim \delta t$ . The optimal measurement time is determined by a trade-off between those two factors. The total estimation error  $\delta \vec{b} = \delta \vec{b}_{\text{stat}} + \delta \vec{b}_{\text{sys}}$  is minimized when they are both of comparable magnitude  $\frac{1}{\sqrt{N \delta t}} \sim \delta t$ , which occurs at an optimal measurement time scaling with the number of experiments as  $\delta t^* \sim N^{-1/4}$ .

The  $N^{-1/4}$  scaling can be understood intuitively as follows. To achieve a reconstruction which is twice more accurate, the total estimation error must be reduced by a factor of 2. This requires measuring at a time shorter by a factor of 2; however, to reduce the statistical error  $\|\delta \vec{b}_{\text{stat}}\| \sim \frac{1}{\sqrt{N \delta t}}$  by a factor of 2 at this twice shorter measurement time, the measurements must be 4 times more accurate, which requires a number of shots which is 16 times larger.

To estimate the optimal  $\delta t^*$  more accurately, we analyze in Appendix A the contributions of the statistical and systematic errors to the reconstruction error,

$$\|\delta \vec{c}\| = \left\| K^+ (\delta \vec{b}_{\text{stat}} + \delta \vec{b}_{\text{sys}}) \right\|. \quad (10)$$

Since the statistical error averages to zero, we find that these contributions factorize, and to leading order in  $\delta t$ ,

$$\begin{aligned} \mathbb{E} \|\delta \vec{c}\|^2 &= \mathbb{E} \left\| K^+ \delta \vec{b}_{\text{stat}} \right\|^2 + \left\| K^+ \delta \vec{b}_{\text{sys}} \right\|^2 \\ &\approx \frac{a_{\text{stat}}}{N(\delta t)^2} + a_{\text{sys}}(\delta t)^2, \end{aligned} \quad (11)$$

for suitable constants  $a_{\text{stat}}$  and  $a_{\text{sys}}$ . The optimal time  $\delta t^*$ , and the corresponding optimal reconstruction error  $\Delta^*$  are therefore approximated by

$$\delta t^* \approx \left( \frac{a_{\text{stat}}}{a_{\text{sys}} N} \right)^{\frac{1}{4}}, \quad \Delta^* \approx \left( 4 \frac{a_{\text{stat}} a_{\text{sys}}}{N} \right)^{\frac{1}{4}} / \|\vec{c}\|. \quad (12)$$

The statistical component  $a_{\text{stat}}$  determines how finite sampling errors degrade the reconstruction. We find that it is given by the spectrum of  $\frac{1}{\sqrt{N_{\text{spam}}}} K$ , which quantifies the sensitivity of the SPAM settings to all the Hamiltonian parameters, averaged over the  $N_{\text{spam}}$  SPAM settings,

$$a_{\text{stat}} = \text{Tr} \left( \left( \frac{1}{N_{\text{spam}}} K^T K \right)^{-1} \right). \quad (13)$$

The systematic component of the error stems from the higher-order derivatives of the estimated observables. When the systematic error is calculated to leading order in  $\delta t$ , it is given by

$$a_{\text{sys}} = \left\| K^+ \partial_{tt} \langle \vec{A} \rangle |_{t=0} \right\|^2, \quad (14)$$

where  $\partial_{tt} \langle A \rangle = -\langle [H, [H, A]] \rangle$ . A more accurate estimate for long times (small  $N$ ) can be calculated using

higher orders derivatives (e.g. using  $\partial_{ttt} \langle A \rangle$  as well, see Appendix A 2). Since the systematic error depends on the unknown Hamiltonian we wish to reconstruct, it must be estimated separately; for instance, by computing it with respect to a guess of the true Hamiltonian.

Remarkably, a rough guess of the true Hamiltonian provides an excellent estimate for the reconstruction error and optimal measurement time. We estimated these quantities for the experiments presented in Fig. 1, using the second-order estimate for the systematic error  $a_{sys}$  described in Appendix A 2. We assumed that the true Hamiltonian is known to an accuracy of 10%, and estimated  $a_{sys}$  according to a perturbed version of the true Hamiltonian

$$H + H' = \sum_j c_j (1 + e_j) S_j, \quad (15)$$

where  $e_j \sim N(0, 0.1^2)$ . Plugged in Eq. (12), this estimate reproduced the reconstruction error in Fig. 1 near its optimum to an excellent accuracy (Fig. 1, left, gray line). The predicted optimal measurement time matched the empirical optimum even at moderate measurement budgets  $N$ . While it is tempting to improve the reconstruction using higher order finite difference methods [45], our experiments found an advantage for these methods only at impractical measurement budgets  $N \geq 10^{11}$  (see Appendix A 3).

*System size scaling.* So far, we numerically estimated the reconstruction error at a fixed number of SPAM settings  $N_{spam} = 648$  and system size  $n = 7$ . How many SPAM settings  $N_{spam}$  are required for reconstruction, and how does the measurement budget  $N$  required for reconstruction scale with system size?

We repeated the reconstruction experiment of random 2-ranged Hamiltonians [Eq. (8)] with varying numbers of different SPAM settings  $N_{spam}$  and a constant total budget of measurements  $N$ . The reconstruction error saturated at  $N_{spam}^* \approx 10^3$  SPAM settings (Fig. 2, left, dots). Crucially, both  $N_{spam}^*$  and the reconstruction error remained unchanged when we increased the system size from  $n = 5$  to  $n = 11$ , keeping the total measurement budget fixed. The larger system yielded the same reconstruction error, saturating at the same number of SPAM settings.

To understand the saturation of the reconstruction error as a function of the number of SPAM settings  $N_{spam}$ , we consider the  $N_{spam} \rightarrow \infty$  limit of all SPAM settings. Averaging over all product states and measurement bases, the correlation matrix  $\frac{1}{N_{spam}} K^T K$  converges to a diagonal matrix with system size independent entries (see Appendix B). The entry for each Hamiltonian term depends only on its support and on the set of measured observables. For example, if only single-site observables  $A_\beta$  are used,

$$\frac{1}{N_{spam}} (K^T K)_{j,j'} \xrightarrow{p \rightarrow \infty} 4 \cdot \frac{2k_j}{3^{k_j+1}} \delta_{j,j'}, \quad (16)$$

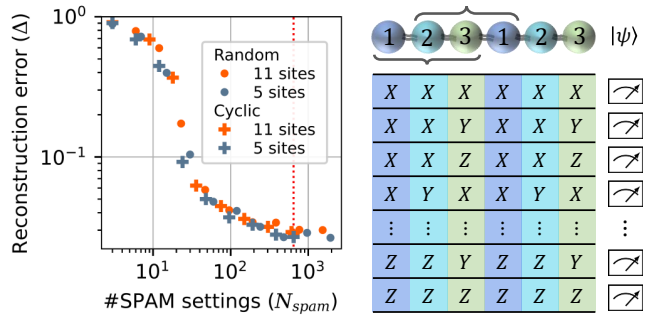


FIG. 2. Left: Reconstruction error as a function of the number of different state preparation and measurement (SPAM) settings for various system sizes and a fixed total number of shots ( $N = 8 \cdot 10^6$ ). The reconstruction accuracy saturates with sufficiently many random SPAM settings, and does not depend on system size (dots). Crosses correspond to random subsets of the cyclic SPAM settings. As the subsets grow to the full set of  $N_{spam} = 6^3 \cdot 3$  cyclic settings (vertical dotted line), they converge to the same reconstruction accuracy as the random settings, explaining the saturation and system-size independence. Right: the measurements of the cyclic protocol (Overlapping Local Tomography). Partition the lattice to unit cells of length  $k$ , then measure each unit cell in an informationally complete set of bases ( $3^k$  in one dimension) to obtain its reduced density matrix, repeating the bases periodically across unit cells. The reduced density matrices of overlapping partitions (gray braces) are obtained for free, since the measurement bases of the different partitions are equal up to a permutation. Initial states in the cyclic measurement scheme are chosen similarly.

where  $k_j$  is the weight of the corresponding Hamiltonian term  $S_j$ , which is the size of its support.

The insensitivity of the reconstruction to system size is apparent in the  $N_{spam} \rightarrow \infty$  average over SPAM settings [Eq. (16)]. The system-size independence of the correlation matrix entries implies a system-size independent statistical error [Eq. (13)] per Hamiltonian term, as the number of Hamiltonian terms is proportional to system size  $L$ . The systematic error [Eq. (14)] per Hamiltonian term is also constant for short-ranged Hamiltonians, since each Hamiltonian term affects a fixed number of observables.

More generally, the system-size independence follows from the local structure of the reconstruction algorithm, since the equations for each Hamiltonian term involve only observables in its vicinity [43]. This local structure also implies that the  $N_{spam} \rightarrow \infty$  limit of Eq. (16) does not require all SPAM settings; only the local configuration of each initial state and measurement basis matters. To predict the number of SPAM configurations required to saturate the reconstruction error, we now devise a structured SPAM scheme. This structured scheme uses a finite number of 'cyclic' SPAM configurations which are equivalent to the  $N_{spam} \rightarrow \infty$  average over all configurations.

The cyclic measurement bases of the structured scheme

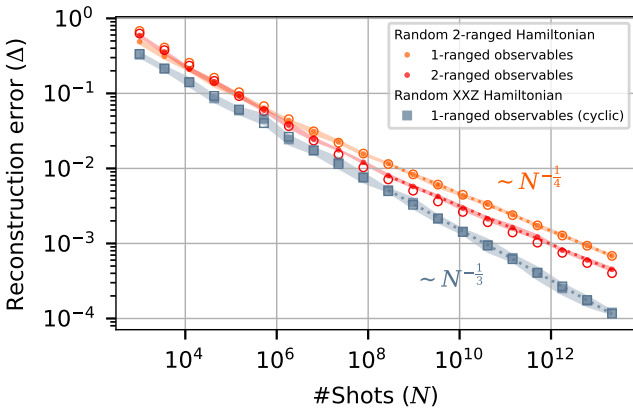


FIG. 3. Reconstruction error as a function of the total number of shots. Warm colors: reconstruction of random 2-ranged Hamiltonians using all observables up to range  $k_\beta$  for  $k_\beta = 1, 2$ . Addition of 2-ranged observables improves the reconstruction accuracy at the same measurement budget  $N$ . Blue: reconstruction of random XXZ Hamiltonians using 1-ranged constraints in a cyclic measurement scheme with periodicity 2. Symmetries of the XXZ model lead to an easier reconstruction, with error scaling asymptotically as  $N^{-1/3}$  in contrast to the  $N^{-1/4}$  scaling predicted for generic Hamiltonians.

are chosen to estimate all observables of a constant range  $k_\beta$  in a given initial state. We construct these measurement by partitioning the lattice to unit cells of length  $k_\beta$ , and iterating over all measurement configurations within a unit cell (Fig. 2, right). The configurations are copied between unit cells, defining a set of  $3^{k_\beta}$  measurement bases in one dimension, or  $3^{k_\beta}$  bases in a  $D$ -dimensional lattice, independent of system size. Inspired by Ref. [50], we call this measurement process 'Overlapping local tomography', since it characterizes all the  $k_\beta$ -ranged reduced density matrices of a given state.

The cyclic initial states are constructed similarly to the cyclic measurement bases. For the purposes of reconstructing a  $k$ -ranged Hamiltonian, cyclic initial states with periodicity  $2k - 1$  are equivalent to the full set of initial product states. This periodicity is chosen to uniformly cover the shared support of every pair of overlapping Hamiltonian terms  $S_i, S_j$  (see Appendix B). For the  $k = 2$ -ranged Hamiltonians and 1-ranged observables considered so far, this structured scheme consists of  $648 = 6^3 \cdot 3$  SPAM configurations, corresponding to the saturation point of Fig. 2. These structured configurations yield a similar reconstruction accuracy as the random configurations (Fig. 2, left, crosses).

*Choosing the observables.* An important factor in the reconstruction is the choice of observables  $\{A_\beta\}$  used for building the linear equation Eq. (5). Each measurement setting can be used to estimate  $2^n - 1$  commuting Pauli observables. Our previous simulations used only single-site observables in the reconstruction. How does the choice of estimated observables affect the reconstruction

quality?

To test this, we repeated our simulations with different choices of observables. We used a fixed set of experimental outcomes to estimate all observables up to range  $k_\beta$  for  $k_\beta = 1, 2, 3$ . While reconstruction with  $k_\beta = 1$  observables was improved by the addition of  $k_\beta = 2$  observables (Fig. 3, warm colors), the addition of  $k_\beta = 3$  degraded the reconstruction (not shown). Correlations between estimated observables cause the degradation for  $k_\beta = 3$ , as well as the deviation between predicted and measured errors for  $k_\beta = 2$  (see Appendix A 1); we conjecture that observables up to a range matching that of the Hamiltonian  $k_\beta = k$  are optimal more generally.

*Symmetry eases Hamiltonian reconstruction.* In contrast to the Hamiltonians we simulated so far, realistic Hamiltonians are not fully random and often have symmetries. How does symmetry affect the reconstruction quality and the accuracy of the our predictions?

To address this question, we repeated our experiments with random XXZ Hamiltonians:

$$H_{XXZ} = \sum_{i=0}^{n-1} c_i Z_i Z_{i+1} + a_i (X_i X_{i+1} + Y_i Y_{i+1}), \quad (17)$$

where  $c_i, a_i \sim N(0, 1)$  are drawn from a Gaussian distribution. These XXZ Hamiltonians are invariant under three anti-unitary symmetries  $\forall i : \sigma_i^\alpha \mapsto -\sigma_i^\alpha$ , each of which flips one of the Bloch axes  $\alpha$  for all spins  $i$  [53]. Interestingly, the reconstruction error of these Hamiltonians in a cyclic measurement scheme decreased more rapidly with the total number of shots  $\Delta \sim N^{-1/3}$  compared to the naive prediction  $N^{-1/4}$  of Eq. (12) (Fig. 3, blue). We find that for initial states that respect at least one of the anti-unitary symmetries of the Hamiltonian, the systematic error  $a_{sys}$  [Eq. (14)] vanishes to first order (see Appendix C). As a result, the systematic error scales as  $\|\delta \vec{b}_{sys}\| \sim \mathcal{O}(\delta t^2)$  instead of  $\mathcal{O}(dt)$ , explaining the  $N^{-1/3}$  scaling of the reconstruction error.

*Conclusions.* We have shown that a system-size independent number of short-time measurements fully characterizes short-ranged Hamiltonians to any given accuracy. Fixing the total number of experimental shots, the error decreases with the number of experimental configurations up to a saturation point. While the error is very sensitive to the measurement time, the optimal time can be predicted using minimal prior knowledge.

Short time measurements for Hamiltonian reconstruction benefit from computational and analytical tractability, as well as favorable system-size scaling. However, the reconstruction scales poorly with the number of shots, since the derivative estimation requires evolution times which decrease with the desired reconstruction accuracy. Longer measurement times can be utilized by substituting the differential Ehrenfest equation [Eq. (2)] by an integral equation for the dynamics of observables over a time period. Alternatively, a higher-order Taylor expansion of the observable dynamics would lead to a non-linear set of equations, which would allow longer mea-

surement times at the cost of computational effort as in the recent Ref. [54]. The optimal measurement time for these higher order methods can be estimated using extensions of the method we presented here.

## ACKNOWLEDGMENTS

We thank Tasneem Watad, Itai Arad and Barak Gur for useful discussions. We acknowledge financial support from the European Research Council (ERC) under the European Union Horizon 2020 Research and Innovation Programme (Grant Agreement No. 639172), the Defense Advanced Research Projects Agency through the DRINQS program, grant No. D18AC00025, and from the Israel Science Foundation within the ISF-Quantum program (Grant No. 2074/19). The content of the information presented here does not necessarily reflect the position or the policy of the U.S. government, and no official endorsement should be inferred.

## I. BIBLIOGRAPHY

- [1] H. Y. Kwon, H. G. Yoon, C. Lee, G. Chen, K. Liu, A. K. Schmid, Y. Z. Wu, J. W. Choi, and C. Won, *Science Advances* **6** (2020), 10.1126/sciadv.abb0872.
- [2] D. Wang, S. Wei, A. Yuan, F. Tian, K. Cao, Q. Zhao, Y. Zhang, C. Zhou, X. Song, D. Xue, and S. Yang, *Advanced Science* **7** (2020), 10.1002/advs.202000566.
- [3] H. Li and F. D. Haldane, *Physical Review Letters* **101** (2008), 10.1103/PhysRevLett.101.010504.
- [4] X. Turkeshi, T. Mendes-Santos, G. Giudici, and M. Dalmonte, *Physical Review Letters* **122** (2019), 10.1103/PhysRevLett.122.150606.
- [5] G. Giudici, T. Mendes-Santos, P. Calabrese, and M. Dalmonte, *Physical Review B* **98** (2018), 10.1103/PhysRevB.98.134403.
- [6] W. Zhu, Z. Huang, and Y. C. He, *Physical Review B* **99** (2019), 10.1103/PhysRevB.99.235109.
- [7] M. Dalmonte, B. Vermersch, and P. Zoller, *Nature Physics* **14** (2018), 10.1038/s41567-018-0151-7.
- [8] C. Kokail, R. van Bijnen, A. Elben, B. Vermersch, and P. Zoller, “Entanglement hamiltonian tomography in quantum simulation,” (2020).
- [9] N. Boulant, T. F. Havel, M. A. Pravia, and D. G. Cory, *Physical Review A - Atomic, Molecular, and Optical Physics* **67**, 12 (2003).
- [10] L. Innocenti, L. Banchi, A. Ferraro, S. Bose, and M. Paternostro, *New Journal of Physics* **22** (2020), 10.1088/1367-2630/ab8aaf.
- [11] E. Ben Av, Y. Shapira, N. Akerman, and R. Ozeri, *Physical Review A* **101** (2020), 10.1103/PhysRevA.101.062305.
- [12] J. Carrasco, A. Elben, C. Kokail, B. Kraus, and P. Zoller, *PRX Quantum* **2**, 010102 (2021).
- [13] E. Magesan, J. M. Gambetta, and J. Emerson, *Physical Review Letters* **106**, 180504 (2011).
- [14] M. D. Shulman, S. P. Harvey, J. M. Nichol, S. D. Bartlett, A. C. Doherty, V. Umansky, and A. Yacoby, *Nature Communications* **5** (2014), 10.1038/ncomms6156.
- [15] S. Sheldon, E. Magesan, J. M. Chow, and J. M. Gambetta, *Physical Review A* **93** (2016), 10.1103/PhysRevA.93.060302.
- [16] N. Sundaresan, I. Lauer, E. Pritchett, E. Magesan, P. Jurecic, and J. M. Gambetta, *PRX Quantum* **1**, 020318 (2020).
- [17] C.-D. Han, B. Glaz, M. Haile, and Y.-C. Lai, (2021).
- [18] A. Sone and P. Cappellaro, *Phys. Rev. A* **95** (2017), 10.1103/PhysRevA.95.022335.
- [19] J. Zhang and M. Sarovar, *Physical Review Letters* **113**, 080401 (2014).
- [20] J. Zhang and M. Sarovar, *Physical Review A - Atomic, Molecular, and Optical Physics* **91** (2015), 10.1103/PhysRevA.91.052121.
- [21] C. Di Franco, M. Paternostro, and M. S. Kim, *Phys. Rev. Lett.* **102** (2009), 10.1103/PhysRevLett.102.187203.
- [22] D. Burgarth, K. Maruyama, and F. Nori, *Phys. Rev. A* **79** (2009), 10.1103/PhysRevA.79.020305.
- [23] G. O. Samach, A. Greene, J. Borregaard, M. Christandl, D. K. Kim, C. M. McNally, A. Melville, B. M. Niedzielski, Y. Sung, D. Rosenberg, M. E. Schwartz, J. L. Yoder, T. P. Orlando, J. I.-J. Wang, S. Gustavsson, M. Kjaergaard, and W. D. Oliver, (2021).
- [24] S. T. Wang, D. L. Deng, and L. M. Duan, *New Journal of Physics* **17** (2015), 10.1088/1367-2630/17/9/093017.
- [25] A. Valenti, E. van Nieuwenburg, S. Huber, and E. Greplova, *Physical Review Research* **1** (2019), 10.1103/physrevresearch.1.033092.
- [26] S. Krastanov, S. Zhou, S. T. Flammia, and L. Jiang, *Quantum Science and Technology* **4** (2019), 10.1088/2058-9565/ab18d5.
- [27] A. Valenti, G. Jin, J. Léonard, S. D. Huber, and E. Greplova, (2021).
- [28] C. E. Granade, C. Ferrie, N. Wiebe, and D. G. Cory, *New Journal of Physics* **14** (2012), 10.1088/1367-2630/14/10/103013.
- [29] N. Wiebe, C. Granade, C. Ferrie, and D. G. Cory, *Phys. Rev. Lett.* **112** (2014), 10.1103/PhysRevLett.112.190501.
- [30] N. Wiebe, C. Granade, C. Ferrie, and D. G. Cory, *Phys. Rev. A* **89** (2014), 10.1103/PhysRevA.89.042314.
- [31] N. Wiebe, C. Granade, and D. G. Cory, *New Journal of Physics* **17** (2015), 10.1088/1367-2630/17/2/022005.
- [32] J. Wang, S. Paesani, R. Santagati, S. Knauer, A. A. Gentile, N. Wiebe, M. Petruzzella, J. L. O’Brien, J. G. Rarity, A. Laing, and M. G. Thompson, *Nat. Phys.* **13**, 551 (2017).
- [33] G. Bentsen, I.-D. Potirniche, V. B. Bulchandani, T. Scafidi, X. Cao, X.-L. Qi, M. Schleier-Smith, and E. Altman, *Physical Review X* **9**, 041011 (2019).
- [34] Z. Li, L. Zou, and T. H. Hsieh, *Physical Review Letters* **124** (2020), 10.1103/PhysRevLett.124.160502.
- [35] A. Shabani, M. Mohseni, S. Lloyd, R. L. Kosut, and H. Rabitz, *Phys. Rev. A* **84** (2011), 10.1103/PhysRevA.84.012107.
- [36] M. P. Da Silva, O. Landon-Cardinal, and D. Poulin, *Physical Review Letters* **107** (2011), 10.1103/PhysRevLett.107.210404.
- [37] X.-L. Qi and D. Ranard, *Quantum* **3**, 159 (2019).
- [38] E. Chertkov and B. K. Clark, *Physical Review X* **8**, 031029 (2018).
- [39] M. Greiter, V. Schnells, and R. Thomale, *Physical Review B* **98**, 081113(R) (2018).
- [40] K. Rudinger and R. Joynt, *Phys. Rev. A* **92** (2015), 10.1103/PhysRevA.92.052322.

- [41] M. Kieferová and N. Wiebe, *Phys. Rev. A* (2017), [10.1103/PhysRevA.96.062327](https://doi.org/10.1103/PhysRevA.96.062327).
- [42] H. J. Kappen, [arXiv:1803.11278](https://arxiv.org/abs/1803.11278) (2018).
- [43] E. Bairey, I. Arad, and N. H. Lindner, *Physical Review Letters* **122** (2019), [10.1103/PhysRevLett.122.020504](https://doi.org/10.1103/PhysRevLett.122.020504).
- [44] E. Bairey, C. Guo, D. Poletti, N. H. Lindner, and I. Arad, *New Journal of Physics* **22** (2020), [10.1088/1367-2630/ab73cd](https://doi.org/10.1088/1367-2630/ab73cd).
- [45] E. F. Dumitrescu and P. Lougovski, “[Hamiltonian Assignment for Open Quantum Systems](#),” (2019).
- [46] T. J. Evans, R. Harper, and S. T. Flammia, (2019).
- [47] A. Anshu, S. Arunachalam, T. Kuwahara, and M. Soleimanifar, [arXiv](https://arxiv.org/abs/2001.08050) (2020).
- [48] A. Elben, B. Vermersch, C. F. Roos, and P. Zoller, *Physical Review A* **99** (2019), [10.1103/PhysRevA.99.052323](https://doi.org/10.1103/PhysRevA.99.052323).
- [49] H. Y. Huang, R. Kueng, and J. Preskill, *Nature Physics* **16** (2020), [10.1038/s41567-020-0932-7](https://doi.org/10.1038/s41567-020-0932-7).
- [50] J. Cotler and F. Wilczek, *Physical Review Letters* **124** (2020), [10.1103/PhysRevLett.124.100401](https://doi.org/10.1103/PhysRevLett.124.100401).
- [51] G. Garcia-Perez, M. A. C. Rossi, B. Sokolov, E.-M. Borrilli, and S. Maniscalco, *Physical Review Research* **2** (2020), [10.1103/physrevresearch.2.023393](https://doi.org/10.1103/physrevresearch.2.023393).
- [52] X. Bonet-Monroig, R. Babbush, and T. E. O’Brien, *Physical Review X* **10** (2020), [10.1103/PhysRevX.10.031064](https://doi.org/10.1103/PhysRevX.10.031064).
- [53] Meng Cheng, “[Time reversal symmetry of transverse field Ising model](#),” Physics Stack Exchange.
- [54] J. Haah, R. Kothari, and E. Tang, [arXiv](https://arxiv.org/abs/2101.01001) (2021).

## Appendix A: Derivative estimation

### 1. Full derivation of the optimal measurement time

#### a. Full derivation of $\mathbb{E}\|\delta\vec{c}\|$ bound

We want to estimate how  $\delta t$  affects  $\mathbb{E}\|\delta\vec{c}\|$ . The effect of  $\delta t$  on  $\delta\vec{b}$  can be written as sum of two contributions  $\delta\vec{b} = \delta\vec{b}_{sys} + \delta\vec{b}_{stat}$  where

$$\delta b_{sys(\alpha,\beta)} = b_{(\alpha,\beta)} - \frac{\langle A_\beta \rangle_{\psi_\alpha(\delta t)} - \langle A_\beta \rangle_{\psi_\alpha(0)}}{\delta t}, \quad (\text{A1})$$

with expectation values evaluated exactly (in the limit of infinite shots), is the systematic error of the estimation (Eq. (6)) and

$$\delta b_{stat(\alpha,\beta)} = \frac{\delta \langle A_\beta \rangle_{\psi_\alpha(\delta t)}}{\delta t} \sim G\left(0, \frac{1}{\delta t^2} \frac{N_{spam}}{N}\right), \quad (\text{A2})$$

with expectation values estimated using  $\frac{N_{spam}}{N}$  shots, is the statistical error due to finite sampling. Writing  $\delta\vec{c} = K^+ \delta\vec{b} = K^+ (\delta\vec{b}_{stat} + \delta\vec{b}_{sys})$  as sum of two independent errors allows us to find a value for  $\mathbb{E}\|\delta\vec{c}\|^2$  using the following lemma on the expectation value of a quadratic form.

**Lemma A.1.** *Let  $\vec{x}$  be a random vector with mean  $\vec{\mu}$  and covariance matrix  $\Sigma$  then for any  $A \in M_{n,m}(\mathbb{R})$ ,  $\mathbb{E}\|A\vec{x}\|^2 = \text{Tr}(\Sigma A^T A) + \|A\vec{\mu}\|^2$ .*

*Proof.* Note that

$$\|A\vec{x}\|^2 = \vec{x}^T A^T A \vec{x}$$

Because  $\|A\vec{x}\|$  is a scalar, we can write

$$\|A\vec{x}\|^2 = \text{Tr}(\vec{x}^T A^T A \vec{x})$$

Using the cyclic property of the trace

$$\|A\vec{x}\|^2 = \text{Tr}(A^T A \vec{x} \vec{x}^T)$$

As trace and matrix multiplication are essentially additions and scalar multiplications we can write

$$\mathbb{E} \text{Tr}(A^T A \vec{x} \vec{x}^T) = \text{Tr}(A^T A \mathbb{E}(\vec{x} \vec{x}^T))$$

Using the definition of the covariance matrix

$$\mathbb{E}\|A\vec{x}\|^2 = \text{Tr}(A^T A (\Sigma + \vec{\mu} \vec{\mu}^T))$$

and from linearity of the trace

$$\mathbb{E}\|A\vec{x}\|^2 = \text{Tr}(A^T A \Sigma) + \text{Tr}(A^T A \vec{\mu} \vec{\mu}^T)$$

Again from the cyclic properties of the trace and the fact that  $\text{Tr}(\vec{\mu}^T A^T A \vec{\mu}) = \|A\vec{\mu}\|^2$  (as it is a scalar):

$$\mathbb{E}\|A\vec{x}\|^2 = \text{Tr}(\Sigma A^T A) + \|A\vec{\mu}\|^2$$

□

In our case  $\delta\vec{b}$  is a random vector with mean  $\delta\vec{b}_{sys}$  and covariance matrix  $\Sigma_{\delta\vec{b}_{stat}} = \mathbb{E}\delta\vec{b}_{stat}\delta\vec{b}_{stat}^T$ . Using that lemma for  $\mathbb{E}\|\delta\vec{c}\|^2 = \mathbb{E}\|K^+ \delta\vec{b}\|^2$  we can find a bound on  $\mathbb{E}\|\delta\vec{c}\|$  using Jensen inequality  $\mathbb{E}\|\delta\vec{c}\| \leq \sqrt{\mathbb{E}\|\delta\vec{c}\|^2}$ :

$$\mathbb{E}\|\delta\vec{c}\| \leq \sqrt{\text{Tr}\left(\mathbb{E}\left(\delta\vec{b}_{stat}\delta\vec{b}_{stat}^T\right) K^{+T} K^+\right) + \|K^+ \delta\vec{b}_{sys}\|^2}.$$

Assuming each entry of  $\delta\vec{b}_{stat}$  is independent random variable with variance  $\sigma_{(\alpha,\beta)}^2$  and zero mean we get that

$$\mathbb{E}\|\delta\vec{c}\| \leq \sqrt{\text{Tr}\left(\Sigma_{\delta\vec{b}_{stat}} K^{+T} K^+\right) + \|K^+ \delta\vec{b}_{sys}\|^2}, \quad (\text{A3})$$

where  $\Sigma_{\delta\vec{b}_{stat}}$  is diagonal with elements  $\sigma_{(\alpha,\beta)}^2$ . Assuming  $\sigma_{(\alpha,\beta)} \sim \left(\frac{N}{N_{spam}}\right)^{-1/2} \frac{1}{\delta t}$  we can define

$$a_{stat} = \text{Tr}\left(\Sigma_{\delta\vec{b}_{stat}}^* N_{spam} K^{+T} K^+\right)$$

where  $\Sigma_{\delta\vec{b}_{stat}}^* = \frac{N}{N_{spam}} \delta t^2 \Sigma_{\delta\vec{b}_{stat}}$  is a diagonal matrix which is independent of  $N, p, \delta t$  and

$$a_{sys} = \frac{1}{\delta t^2} \|K^+ \delta\vec{b}_{sys}\|^2$$

Assuming  $\delta\vec{b}_{sys} \sim \delta t$  (first order estimation of the systematic error) we get Eq. (11), and if we assume that  $\Sigma_{\delta\vec{b}_{stat}}^* = \mathbb{1}$  (i.e. all the observables have the same statistical error magnitude) using the cyclic property of the trace we can write  $a_{stat} = \text{Tr} \left( N_{spam} (K^T K)^{-1} \right)$ .

In practice, the standard deviations varies between observables depending on the initial state. Moreover, when different observables are estimated from the same set of measurements, off-diagonal entries appear in the covariance matrix. These correlations explain the deviation between the predicted and observed accuracies in Fig. 3. They can be taken into account in order to improve the prediction of the reconstruction, and to predict the optimal set of estimated observables.

### b. Estimating the optimal $\delta t$

In Eq. (11) and subsequent derivations, we have assumed that the statistical error scales as  $\delta\vec{b}_{stat} \propto \left( \frac{N}{N_{spam}} \right)^{-1/2} \delta t^{-1}$  and the systematic error as  $\delta\vec{b}_{sys} \propto \delta t$ . We can examine a more general case with

$$\begin{aligned} \delta\vec{b}_{stat} &= \vec{a}_{stat} \left( \frac{N}{N_{spam}} \right)^{-1/2} \delta t^{-\gamma} \\ \delta\vec{b}_{sys} &= \vec{a}_{sys} \delta t^\lambda + \mathcal{O}(\delta t^{\lambda+1}) \end{aligned}$$

for  $\lambda, \gamma \neq 1$ .  $\vec{a}_{stat}, \vec{a}_{sys}$  are defined such that they are independent of  $\delta t$ . The optimal  $\delta t$  is achieved when  $\mathbb{E} \|\delta\vec{c}\|$  is minimal. As an approximation, we use the bound

$$\|\delta c\|_{bound} = \sqrt{\text{Tr} \left( \Sigma_{\delta\vec{b}_{stat}} K^{+T} K^+ \right) + \left\| K^+ \delta\vec{b}_{sys} \right\|^2} \text{ of Eq. (A3), and minimize it with respect to } \delta t. \text{ To leading order in } \delta t \text{ we get}$$

$$\begin{aligned} \|\delta c\|_{bound}^2 &= \frac{\delta t^{-2\gamma}}{N} \text{Tr} \left( \Sigma_{\vec{a}_{stat}} K^{+T} K^+ \right) \\ &\quad + \delta t^{2\lambda} \left\| K^+ \delta\vec{a}_{sys} \right\|^2. \end{aligned}$$

The derivative is given by

$$\begin{aligned} \frac{d}{d(\delta t)} \|\delta c\|_{bound}^2 &= -2 \frac{\gamma \delta t^{-2\gamma-1}}{N} \text{Tr} \left( \Sigma_{\vec{a}_{stat}} K^{+T} K^+ \right) \\ &\quad + 2\lambda \delta t^{2\lambda-1} \left\| K^+ \delta\vec{a}_{sys} \right\|^2 \end{aligned}$$

The minimum is achieved when the derivative vanishes, which occurs at

$$\delta t^* = \left( \frac{1}{N} \cdot \frac{\gamma \text{Tr} \left( \Sigma_{\vec{a}_{stat}} K^{+T} K^+ \right)}{\lambda \left\| K^+ \delta\vec{a}_{sys} \right\|^2} \right)^{1/2(\gamma+\lambda)}, \quad (\text{A4})$$

which corresponds to reconstruction error

$$\begin{aligned} \|\delta c^*\|_{bound} &= \left( \sqrt{\frac{1}{1-\kappa}} \frac{1}{\sqrt{N}} \sqrt{\text{Tr} \left( \Sigma_{\vec{a}_{stat}} K^{+T} K^+ \right)} \right)^{1-\kappa} \\ &\quad \cdot \left( \sqrt{\frac{1}{\kappa}} \left\| K^+ \delta\vec{a}_{sys} \right\| \right)^\kappa, \quad (\text{A5}) \end{aligned}$$

where  $\kappa = \frac{\gamma}{\lambda+\gamma}$ . This result generalizes Eq. (12), where  $\gamma = \lambda = 1$  and  $\kappa = 1/2$ .

## 2. Estimation used in the Hamiltonian reconstruction simulations

In our simulations, the systematic error due to the finite derivative method was estimated using a perturbed version of the real Hamiltonian, used to calculate the higher derivatives  $\partial_{tt} \langle A_j \rangle_{t=0}$  and  $\partial_{ttt} \langle A_j \rangle_{t=0}$  of the observables. The systematic error is defined as

$$a_{sys} = \left\| K^+ \left( \partial_t \langle \vec{A} \rangle|_{t=0} - \frac{\langle \vec{A} \rangle_{\delta t} - \langle \vec{A} \rangle_0}{\delta t} \right) \right\|^2.$$

Writing  $\langle \vec{A} \rangle_{\delta t}$  as a Taylor expansion around  $t = 0$  gives:

$$\begin{aligned} \langle \vec{A} \rangle_{\delta t} &= \langle \vec{A} \rangle_0 + \delta t \partial_t \langle \vec{A} \rangle|_0 + \frac{\delta t^2}{2} \partial_{tt} \langle \vec{A} \rangle|_0 \\ &\quad + \frac{\delta t^3}{6} \partial_{ttt} \langle \vec{A} \rangle|_0 + \mathcal{O}(\delta t^4) \quad (\text{A6}) \end{aligned}$$

Then for first order in  $\delta t$  the systematic error is:

$$a_{sys} = \left\| K^+ \left( \frac{1}{2} \partial_{tt} \langle \vec{A} \rangle|_{t=0} \right) \right\|^2$$

and for second order in  $\delta t$ :

$$a_{sys} = \left\| K^+ \left( \frac{1}{2} \partial_{tt} \langle \vec{A} \rangle|_{t=0} + \frac{\delta t}{6} \partial_{ttt} \langle \vec{A} \rangle|_{t=0} \right) \right\|^2 \quad (\text{A7})$$

Evaluating this second order estimate for  $a_{sys}$  requires to know  $\delta t$  which is our ultimate goal to find. In order to bypass this difficulty, we used the first order estimate of  $a_{sys}$  in Eq. (12) to get a first order estimate of  $\delta t$ , and used that estimate in the second order estimate of  $a_{sys}$  to get a better prediction of  $\delta t$ .

## 3. Higher order finite difference approximations

Examining the analytical results we got for the reconstruction error bound in Eq. (A5) we can try to improve the reconstruction using higher-order estimates for the derivative. Instead of using the finite difference method

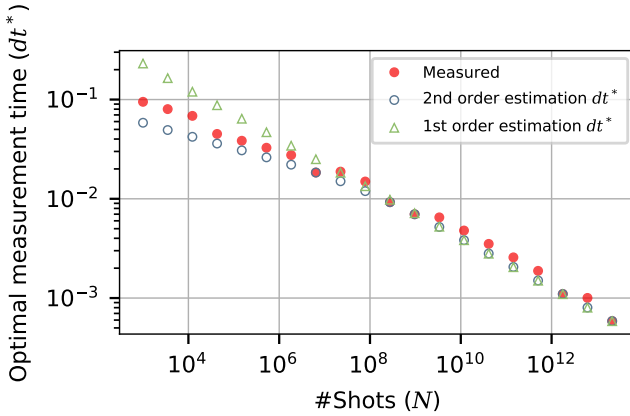


FIG. S4. Predicting the optimal measurement time using first order (green hollow triangles, Eq. (14)) or second order (blue circles, Eq. (A7)) methods in a random 2-local Hamiltonian compared to the measured optimal time (red dots). Here we used 2-ranged observables in a randomized measurement scheme.

with a single forward point (Eq. (6)), we can use forward finite difference method with  $\lambda > 1$  points

$$\partial_t \langle A \rangle_\psi = \frac{\sum_{r=0}^\lambda w_r \langle A \rangle_{\psi(r \cdot \delta t)}}{\delta t} + \mathcal{O}(\delta t^\lambda) \quad (\text{A8})$$

where  $w_r$  are the weights of each point such that the estimation error is  $\mathcal{O}(\delta t^\lambda)$ . In that case we will achieve better asymptotic behaviour with respect to the number of measurements (as  $\|\delta c^*\|_{\text{bound}} \propto \sqrt{N^{\frac{\lambda}{\lambda+1}}}$ , Eq. (A5)) but the measurement budget will split between  $\lambda$  measurement times. The measurement budget at different times can be allocated wisely by finding a set  $\{N_r\}_{r=1}^\lambda; \sum_{r=1}^\lambda N_r = N$  which minimizes the variance of the statistical error  $\sigma^2 = \sum_{r=1}^\lambda w_r^2/N_r$ , which is achieved for

$$N_r = N \frac{|w_r|}{\sum_{r=1}^\lambda |w_r|}. \quad (\text{A9})$$

Hence, the  $N$  used in the statistical error should be replaced with  $N_{\text{effective}} = N \left( \frac{1}{\sum_{r=1}^\lambda |w_r|} \right)^2$ , which yields an additional  $\left( \sum_{r=1}^\lambda |w_r| \right)^{\frac{\lambda}{\lambda+1}}$  factor to the reconstruction error bound because of the statistical error (Eq. (A5)). Additional factors can arise due to the systematic error.

We examined the results of reconstruction using finite difference with  $\lambda = 2$  uniformly spaced forward points

$$\partial_t \langle A \rangle_\psi = \frac{-\frac{3}{2} \langle A \rangle_{\psi(0)} + 2 \langle A \rangle_{\psi(\delta t)} - \frac{1}{2} \langle A \rangle_{\psi(2\delta t)}}{\delta t} + \mathcal{O}(\delta t^2). \quad (\text{A10})$$

Comparing the results we got using 1 forward point finite difference (Eq. (6)) to the results using 2 forward points finite difference (Eq. (A10)) we observed that the scaling advantage from the 2 forward points estimation

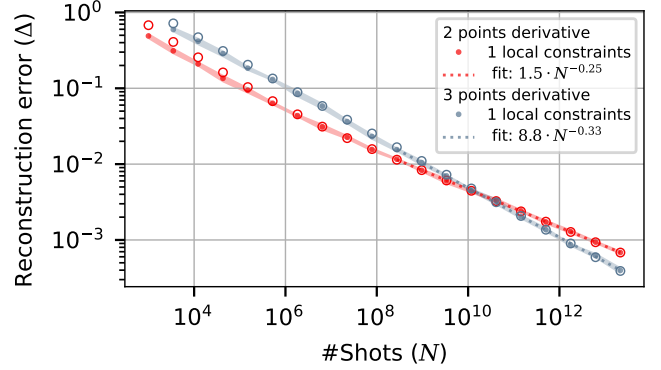


FIG. S5. Reconstruction error of a random 2-local Hamiltonian as a function of the total number of shots using different methods of derivative estimation: 2 points forward finite difference (blue dots, Eq. (6)) and 3 points forward finite difference (red dots, Eq. (A10)).

method yields better reconstruction only for  $N > 10^{11}$  as can be seen in Fig. S5.

## Appendix B: Analytic estimate of the statistical reconstruction error

A unique reconstruction requires a set of initial states and measurement bases leading to a full rank reconstruction matrix  $K$ . More generally, the choice of experiments determines the spectrum of  $K^T K$ , which quantifies the sensitivity of the experiments to the Hamiltonian terms through the statistical error of Eq. (13). We now derive the analytical form of  $K^T K$  when averaged over all experimental configurations, and show that it is sufficient to average over a finite set of local configurations.

For a given set of initial states  $|\psi_\alpha\rangle$  and observables  $A_\beta$ ,

$$(K^T K)_{ij} = - \sum_{\alpha, \beta} \langle i[S_i, A_\beta] \rangle_{\psi_\alpha} \langle i[S_j, A_\beta] \rangle_{\psi_\alpha}, \quad (\text{B1})$$

by the definition of  $K$  [Eq. (3)]. Here,  $A_\beta$  denote all the observables compatible with the measurement basis for the initial state  $|\psi_\alpha\rangle$  up to the chosen locality. When averaging over all possible configurations, each of the  $6^n$  initial states is measured in  $3^n$  measurement bases. However, for a given initial state  $|\psi_\alpha\rangle$ , each observable  $A_\beta$  is compatible with many measurement bases. An observable with support  $s \subseteq [1, \dots, n]$  is compatible with  $\frac{1}{3^{|s|}}$  of all measurement bases; for instance,  $X_1$  is compatible with  $\frac{1}{3}$  of all bases. Therefore, the average  $\frac{1}{N_{\text{spam}}} (K^T K)_{ij}$  over all configurations  $N_{\text{spam}} = \frac{1}{3^n \cdot 6^n}$  takes the form

$$\sum_\beta \frac{1}{3^{|s_\beta|}} \sum_\alpha \frac{1}{6^n} \langle i[S_i, A_\beta] \rangle_{\psi_\alpha} \langle i[S_j, A_\beta] \rangle_{\psi_\alpha}. \quad (\text{B2})$$

where  $\beta$  runs over all estimated observables. We will now show that this average

1. Vanishes for off-diagonal elements where  $S_i \neq S_j$ .
2. For the diagonal element corresponding to  $S_i$ , it counts the number of observables  $A_\beta$  that fail to commute with  $S_i$ , normalized by the weight  $s_\beta$  of  $A_\beta$  and the weight  $s_{i,\beta}$  of the commutator  $[S_i, A_\beta]$ .
3. Depends only on initial state and measurement configurations on sites supported by  $S_i$  or  $S_j$ .
4. Vanishes identically for *any* initial state  $|\psi_\alpha\rangle$  when  $S_i, S_j$  do not overlap at least on one site, so that averaging over  $2k_h - 1$ -local configurations suffices.

For the first two claims, we invoke the following formula for product state averages of Pauli strings [34]:

$$\frac{1}{6^n} \sum_{\alpha} \langle P_r \rangle_{\psi_\alpha} \langle P'_r \rangle_{\psi_\alpha} = \frac{1}{3^{|s_r|}} \delta_{r,r'}, \quad (\text{B3})$$

which states that the average over all initial states vanishes whenever the two Pauli strings are different, and decays with their support  $|s_r|$  otherwise. In our case,  $i[S_i, A_\beta] = 2P_{r_{i,\beta}}$  is a Pauli string since both  $S_i$  and  $A_\beta$  are.

*Off-diagonal terms vanish.* Considering Eq. (B3), it is sufficient to show that different Hamiltonian terms  $S_i \neq S_j$  have different commutators with a shared Pauli observable  $[S_i, A_\beta] \neq [S_j, A_\beta]$ , assuming that both commutators are non-zero. To see this, we recall that any pair of Paulis either commutes or anticommutes. Therefore, if  $[S_i, A_\beta] \neq 0$ , we can write  $[S_i, A_\beta] = \theta_{i,\beta} S_i A_\beta$  for some  $\theta_{i,\beta} \neq 0$ , and similarly for  $S_j$ . If  $[S_i, A_\beta] = [S_j, A_\beta]$ , then  $\theta_{i,\beta} S_i A_\beta = \theta_{j,\beta} S_j A_\beta$ , and  $S_i = \theta_{i,\beta}^{-1} \theta_{j,\beta} S_j$ , in contradiction to our assumption.

*Diagonal elements count non-commuting observables.* For diagonal elements  $i = j$ , Eq. (B3) gives a positive contribution whenever  $[S_i, A_\beta] \neq 0$ . The average over initial states  $\alpha$  yields a contribution  $\frac{4}{3^{|s_{i,\beta}|}}$  which depends only on the size of the support  $s_{i,\beta}$  of the commutator  $[S_i, A_\beta]$ , such that Eq. (B2) becomes

$$\sum_{A_\beta: [S_i, A_\beta] \neq 0} \frac{4}{3^{|s_\beta| + |s_{i,\beta}|}}, \quad (\text{B4})$$

where the sum runs over all observables  $A_\beta$  up to the chosen observable locality that fail to commute with  $S_i$ , and the factor 4 comes from the two commutators. For example, for single-site  $S_i$  and  $A_\beta$  we get  $4 \cdot \frac{2}{9}$ , since  $\frac{2}{3}$  of all single-site Paulis  $A_\beta$  fail to commute with a single-site Hamiltonian Pauli  $S_i$ ; and  $\frac{1}{3}$  of the Pauli measurement bases match each given commutator.

More generally, since our measurement bases average equally over all observables  $A_\beta$  with the same support, the value of Eq. (B2) depends only on the support of  $S_i$ , i.e. its locality and range. It can be calculated explicitly for a given set of estimated observables  $A_\beta$ .

*Only local configurations matter.* We now show that for each  $i, j$ , Eq. (B2) depends only on local configurations within the support of  $S_i$  and  $S_j$ . Namely, it does not depend on the initial state configuration on sites supported by the observable  $A_\beta$  but not by any of the Hamiltonian terms. We assume that all observables  $A_\beta$  with a given support are sampled equally, as in the overlapping local tomography ('cyclic') measurement scheme.

Consider a fixed initial state  $|\psi_\alpha\rangle$ , and the average over all observables  $A_\beta$  with a given support  $s$ :

$$\frac{1}{3^{|s|}} \sum_{A_\beta: \text{supp}(A_\beta) = s} \langle i[S_i, A_\beta] \rangle_{\psi_\alpha} \langle i[S_j, A_\beta] \rangle_{\psi_\alpha}. \quad (\text{B5})$$

The Paulis of  $A_\beta$  on the sites are untouched by  $S_i$  or  $S_j$  factor out of both commutators. When we average over all observables with the same support, only a single observable configuration on those sites matches the initial state  $|\psi_\alpha\rangle$ , regardless of the initial state or Hamiltonian terms. Formally, we split  $A_\beta$  to the part that intersects  $S_i$  or  $S_j$  and the part that does not,

$$A_\beta = A_\beta^{s \cap s_{ij}} \cdot A_\beta^{s \setminus s_{ij}} = \prod_{i=1}^{|s \cap s_{ij}|} \sigma_{m_i}^{\beta_{m_i}} \prod_{i=|s \cap s_{ij}|+1}^{|s|} \sigma_{m_i}^{\beta_{m_i}} \quad (\text{B6})$$

where  $m$  is a site index,  $\beta_m \in \{X, Y, Z\}$  is a Pauli index, and  $s_{ij} \stackrel{\text{def}}{=} \text{supp}(S_i) \cup \text{supp}(S_j)$ . We can then write Eq. (B5) as

$$\frac{1}{3^{|s|}} \sum_{\beta_{m_1}, \dots, \beta_{m_{|s \cap s_{ij}|}}} \langle i[S_i, A_\beta^{s \cap s_{ij}}] \rangle_{\psi_\alpha} \langle i[S_j, A_\beta^{s \cap s_{ij}}] \rangle_{\psi_\alpha}. \quad (\text{B7})$$

$$\cdot \sum_{\beta_{|s \cap s_{ij}|+1}, \dots, \beta_{|s|}} \langle A_\beta^{s \setminus s_{ij}} \rangle_{\psi_\alpha}^2. \quad (\text{B8})$$

For any given initial state, the second sum over all observable configurations that are untouched by  $S_i$  or  $S_j$  gives 1. Since the first sum depends only on the initial state configurations in  $s \cap s_{ij}$ , it is sufficient to average over those.

*Distant off-diagonal terms vanish for any product state.* We now show that  $(K^T K)_{ij}$  vanishes for each of our initial states whenever  $S_i, S_j$  do not overlap. For a given Pauli observable  $A_\beta$ , we done its part that intersects  $S_i$  by  $A_\beta^{s_i}$ ; namely, we partition  $A_\beta$  to

$$A_\beta = A_\beta^{s_i} \cdot A_\beta^{s \setminus s_i}. \quad (\text{B9})$$

If  $A_\beta$  commutes with  $S_i$ , its contribution to Eq. (B2) vanishes. To have a non-vanishing contribution, it must anticommute with  $S_i$ , since Pauli strings either commute or anticommute. In this case, we must have that  $A_\beta^{s_i}$  anticommutes with  $S_i$ , since  $A_\beta^{s \setminus s_i}$  trivially commutes with it. However,  $A_\beta^{s_i}$  commutes with  $S_j$ , since they do not

overlap. Therefore, since expectation values in product states factorize,

$$\langle i[S_i, A_\beta] \rangle_{\psi_\alpha} \langle i[S_j, A_\beta] \rangle_{\psi_\alpha} = \quad (B10)$$

$$= \langle i[S_i, A_\beta^{s_i}] \rangle \langle A_\beta^{s \setminus s_i} \rangle \langle A_\beta^{s_i} \rangle \langle i[S_i, A_\beta^{s \setminus s_i}] \rangle. \quad (B11)$$

This product includes the expectation values of anticommuting Pauli strings:  $A_\beta^{s_i}$  anticommutes with  $i[S_i, A_\beta^{s_i}]$ , since we assumed it anticommutes with  $S_i$ . As our initial states are stabilizer states, their expectation value cannot be non-zero for a pair of anticommuting Pauli strings, leading to a vanishing contribution to Eq. (B2) for *any* Pauli observable  $A_\beta$ .

*2k<sub>h</sub> – 1-local configurations suffice.* We have shown that for pair of Hamiltonian terms  $S_i, S_j$ , it is sufficient to sample local configurations on their shared support; and that it is sufficient to consider Hamiltonian terms that intersect. Therefore,  $\frac{1}{N_{spam}} K^T K$  becomes diagonal with entries described by Eq. (B4) if all the local initial state configurations are uniformly sampled within any  $2k_h$  – 1-ranged patch.

### 1. Examples for diagonal entry calculations

We would like to evaluate the diagonal entries of  $\frac{1}{N_{spam}} K^T K$  in the limit of all SPAM settings  $N_{spam} \rightarrow \infty$  [Eq. (B1)] for a few simple cases: (i) 1-local observables and generic Hamiltonian terms, corresponding to the result of Eq. (16) and (ii) 1-local Hamiltonian terms and generic observables.

The diagonal entry for a Hamiltonian term  $S_i$  [Eq. (B4)] counts the number of measured observables that do not commute with it, normalized by the weight of the observable and of the commutator. For instance, each 1-local observable  $A_\beta$  is compatible with one third of all measurement bases, yielding a normalization factor  $\frac{1}{3}$  for the observable locality ( $s_\beta = 1$ ). Given a weight  $k_i$  Hamiltonian term  $S_i$ , any non-zero commutator  $[S_i, A_\beta]$  is itself of weight  $k_i$ , vanishing in all but  $\frac{1}{3^{k_i}}$  of all initial states ( $s_{i,\beta} = k_i$ ). Finally, for each of the  $k_i$  sites in the support of  $S_i$  there are two single-site Paulis that differ from it on that site, yielding a combinatorial factor of  $2k_i$  non-commuting observables. We conclude that

$$\frac{1}{N_{spam}} (K^T K)_{ii} = \sum_{A_\beta: [S_i, A_\beta] \neq 0} \frac{4}{3^{|s_\beta| + |s_{i,\beta}|}}, = 4 \cdot \frac{2k_i}{3^{k_i+1}}.$$

As another example, we examine the case of a 1-local Hamiltonian term  $k_i = 1$  and range  $k_\beta$  observables in a one-dimensional chain with periodic boundary conditions. In that case  $|s_\beta| = |s_{i,\beta}|$ . For  $k_\beta = 2$ -ranged observables,

$$\frac{1}{N_{spam}} (K^T K)_{ii} = \frac{4}{3^{2+2}} \cdot 2 \cdot 2 \cdot 3 = 4 \cdot \frac{4}{3^3}. \quad (B12)$$

The combinatorial factor consists of three contributions: 2 possible Pauli operators that anticommute with  $S_i$  on the site that intersects with it; 2 possible choices of a neighboring site for the observable support; and 3 possible Pauli operators on the neighboring site. Similarly, for  $k_\beta = 3$ -ranged observables,  $\frac{1}{N_{spam}} (K^T K)_{ii} = \frac{4}{3^{3+3}} \cdot 2 \cdot 3 \cdot 3^2 + \frac{4}{3^{2+2}} \cdot 2 \cdot 2 \cdot 3 = 4 \cdot \frac{18}{3^4}$ . The left term counts the observables with both range and weight 3, while the right term counts observables with range 3 and weight 2.

The Table below sums results for  $\frac{1}{4p} (K^T K)_{ii}$  with up to range 3 observables and weight 3 Hamiltonian terms:

$k_\beta \backslash k_i$	1	2	3
1	$2/3^2$	$4/3^3$	$18/3^4$
2	$4/3^3$	$16/3^4$	$52/3^5$
3	$6/3^4$	$28/3^5$	$114/3^6$

The first column and row are the examples calculated above. The columns denote the contribution of all the observables with exact range  $k_\beta$  to the diagonal entry. In the rows, we consider terms acting nontrivially on each of  $k_i$  contiguous sites, such that  $k_i$  denotes both the weight and range of the  $S_i$  term. This assumption is not necessary for  $k_\beta = 1$ , where the result depends only on the weight of  $S_i$ .

### 2. Cyclic measurement scheme in higher-dimensional lattices

How many copies of a state  $|\psi\rangle$  on a  $d$ -dimensional lattice do we need to measure each  $k$ -ranged observable at least once? In 1D we defined a unit cell of length  $k$ . To measure all the  $k$ -ranged observables, it sufficed to iterate over the  $3^k$  Pauli bases of a single unit cell, repeating measurement bases between different unit cells. Since different unit cell partitions are equivalent up to a permutation, this process yields at least one shot of each observable using exactly  $3^k$  copies of the state.

We can generalize this approach to  $d$ -dimensional lattices. We choose a  $d$ -dimensional square unit cell of side length  $k$ , containing  $k^d$  sites (see 2D case in Fig. S6). As in the 1D case, we evaluate all the  $k$ -local observables within it using  $3^{(k^d)}$  different copies, repeating the measurement bases between unit cells. This procedure yields at least one sample of any observable residing within length  $k$  cube, even if it does not respect the original lattice partition. Similarly, since there are 6 Pauli eigenstates per site,  $6^{k^d}$  initial states cover all the Pauli eigenstates in each length  $k$  cube.

The local measurement process we described improves upon the overlapping tomography protocol of Ref. [50] for the special case of geometrically local lattices. The protocol of Ref. [50] recovers all  $k$ -local observables (maximal weight  $k$ ) without assuming any spatial structure. The protocol requires  $\mathcal{O}(\log^2 n)$  copies of a state of  $n$  qudits to recover all observables of a fixed locality to

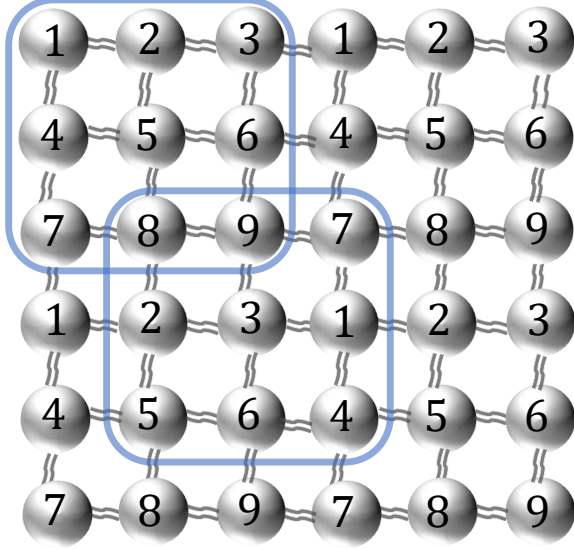


FIG. S6. Example of overlapping tomography (cyclic method) in a  $d = 2$  dimension square lattice with  $k_\beta = 3$ . The boundary of unit cells is colored in blue for two of the unit cells. In this example we need  $3^9$  copies of  $|\psi\rangle$  to get one sample of every 3-ranged observable in the system.

a given worst-case error. Our protocol requires an  $n$ -independent number of copies to recover all short-ranged observables to a constant average accuracy. It effectively eliminates one  $\log n$  factor, which is required in order to cover all long-ranged observables. The other  $\log n$  factor stems only from the different error metric (worst-case vs. average-case).

### Appendix C: XXZ model

Why does the reconstruction error for the  $XXZ$  Hamiltonians of Eq. (17) decrease more rapidly with the measurement count  $\Delta \sim N^{-1/3}$  compared to the  $N^{-1/4}$  scaling of generic 2-local Hamiltonians?

Since the  $XXZ$  Hamiltonians are real in the computational basis, they are invariant under the anti-unitary complex conjugation operator which flips  $Y_i \mapsto -Y_i$  [53]. As these Hamiltonians contain only even combinations of the other Paulis  $X, Z$  as well, they are actually invariant under a time-reversal symmetry for each axis  $\alpha = 1, 2, 3$  of the Bloch sphere, which flips  $\sigma_i^\alpha \mapsto -\sigma_i^\alpha$ .

Incidentally, each of the 2-periodic cyclic initial states we have chosen in Fig. 3 is invariant under one of those symmetries, as the spins of each of these states are po-

larized only within a plane in the Bloch sphere. In other words, each of these states contains only two of the three Paulis, and is invariant under an inversion of the third. We now explain why this implies that for any Pauli observable  $A$ , either (i) the time derivative vanishes  $\partial_t \langle A \rangle = 0$ , or (b) the second time-derivative vanishes  $\partial_{tt} \langle A \rangle = 0$ .

Without loss of generality, we focus on the  $Y \mapsto -Y$  time reversal symmetry, and consider a real-valued initial state which is invariant under the standard complex conjugation, such as  $|\psi\rangle = |\uparrow\uparrow\uparrow\cdots\rangle$ . Each Pauli observable  $A$  has a definite parity under this symmetry: it is either real (even) or purely imaginary (odd), depending on the parity of its number of  $Y$  operators. Since the Hamiltonian is real, it flips the parity of  $A$  under Heisenberg evolution: if  $A$  is real, then  $\partial_t A = i[H, A]$  is imaginary and vice versa.

Importantly, if an observable  $O$  and a state  $\rho$  have definite time reversal parities, they must match for the observable to take an expectation value. If  $\rho$  is a real density matrix and  $O$  an imaginary observable, then

$$\begin{aligned} \text{Tr}(\rho O) &= \text{Tr}((\rho O)^T) = \text{Tr}(\rho^T O^T) \\ &= -\text{Tr}(O\rho) = -\text{Tr}(\rho O), \end{aligned}$$

since  $O^T = (O^\dagger)^* = O^* = -O$ , and the trace of any operator is the same as the trace of its transpose.

Therefore, only time-reversal odd observables  $A$  contribute to the reconstruction in a time-reversal even initial state. If  $A$  is time-reversal even, then  $\partial_t A = i[H, A]$  is time-reversal odd; in this case,  $\partial_t \langle A \rangle_\psi$  vanishes for a time-reversal even state  $|\psi\rangle$  regardless of the particular coefficients of the  $XXZ$  Hamiltonian. In contrast, time-reversal odd observables  $A$  have a non-trivial time derivative, since  $\partial_t A$  is time-reversal even; however, in this case  $\partial_{tt} A = -[H, [H, A]]$  is again time reversal odd, so that  $\partial_{tt} \langle A \rangle = 0$ , and the systematic error [Eq. (A1)] vanishes to first order in  $\delta t$ . Therefore, the time-reversal odd observables  $A$  that participate in the reconstruction can be measured at later times compared to a generic Hamiltonian, leading to an improved scaling of the reconstruction error  $N^{-1/3}$  according to Eq. (A5).

This analysis holds for every Pauli observable in a state whose spins are polarized along the  $X-Z$  plane, based on the  $Y \mapsto -Y$  symmetry. Since the  $XXZ$  Hamiltonian is invariant under inversion of any axis of the Bloch sphere, it generalizes to any initial state whose spins are polarized along a plane. The 2-periodic initial states satisfy this condition, explaining the findings of Fig. 3. More generally, if a Hamiltonian has time-reversal symmetry along one axis, initial states polarized along the perpendicular plane will yield the improved scaling of the reconstruction error.